Applied Surface Science 277 (2013) 40–46

Contents lists available at SciVerse ScienceDirect

Applied Surface Science

journal homepage: www.elsevier.com/locate/apsusc

Effects of catalyst characters on the photocatalytic activity and process of NiO nanoparticles in the degradation of methylene blue

Xia Wan[a,1], Meng Yuan[a], Shao-long Tie[a,*], Sheng Lan[b]

[a] School of Chemistry and Environment, South China Normal University, Guangzhou 510006, PR China
[b] School of Information and Optoelectronic Science and Engineering, South China Normal University, Guangzhou 510006, PR China

ARTICLE INFO

Article history:
Received 18 December 2012
Received in revised form 28 February 2013
Accepted 19 March 2013
Available online 26 March 2013

Keywords:
Nano-scale NiO
Synthesis condition
Catalyst character
Photocatalysis
Methylene blue degradation

ABSTRACT

By a hydrothermal method combining a subsequent calcination process, series of nano-scale NiO samples with different morphologies and sizes were synthesized and characterized. The effects of synthesis conditions including using different alkali reactants and being calcined at different temperatures on the characters of NiO samples have been investigated. In these characters the integrality of crystal structure and the crystallinity of NiO were found to become the determinative factors which affect the photocatalytic activity and process of NiO catalyst in the degradation of methylene blue (MB). The NiO sample which has a good crystallinity and small particle size (≤100 nm) possesses more shallowly trapped holes to react with chemisorbed oxhydryl OH^- or H_2O to generate $OH^\bullet$ radicals, exhibiting a high photocatalytic activity, furthermore, in this UV/NiO suspension the photocatalytic oxidation process of MB occurrs via the attack by $OH^\bullet$ radicals. The NiO sample which has a higher crystallinity and bigger particle size (>200 nm) possesses more deeply trapped holes (h^+_{vb}) to react directly with physisorbed organism, exhibiting a low photocatalytic activity, therefore, in this system the MB is oxidized by direct reacting with holes (h^+_{vb}).

1. Introduction

In the past two decades, photocatalytic degradation organic pollutant by semiconductor oxide such as TiO_2, ZnO, NiO, SnO_2, Cu_2O, and In_2O_3 has attracted public concern due to their high photocatalytic efficiency, low cost and low toxicity, high physical and chemical stability, especially, strong ability of fully decomposing organic pollutant into harmless species (e.g. CO_2, H_2O, etc.) [1–6]. The photocatalytic degradation mechanism of organic pollutant has been widely demonstrated that when the semiconductor oxide is illuminated with UV or visible light, an electron excites out of its energy level to the conduction band and consequently leaves a hole in the valence band to give a electron (e^-)–hole (h^+) pair. The potential of hole (h^+) is positive enough to react with the adsorbed OH^- or H_2O on oxide surface to generate hydroxyl radicals ($^\bullet OH$), and the potential of electron (e^-) is negative enough to reduce molecular oxygen into superoxide ion ($^\bullet O_2^-$). These active species have capable to degrade toxic compounds into harmless species. Synchronously, the holes (h^+) and electrons (e^-) rapidly recombine each other, inducing the decrease of photocatalytic activity [7–9].

In these semiconductor oxides TiO_2 as a photocatalyst has been widely investigated. NiO is also used as a photocatalyst to decompose organic pollutant. Some studies have attempted to exploit NiO for the capability of efficiently using solar light or visible light [10–12]. Other studies attempted to extend the probability of electron–hole separation to enhance the photocatalytic activity by composing a p–n junction heterogeneous NiO catalyst [13–15]. It has been known that preparation methods of photocatalyst as well as post-treatment conditions strongly affect the characters of catalyst and the photocatalytic performance in the degradation of organic pollutant. In the characters of catalyst, such as morphology and surface peculiarity, particle size, specific surface area, crystallinity and crystal quality, and optical property, which one is a determinative factor in the degradation of organic pollutant and how to affect on photocatalytic activity and mechanism become our concerned issues. To the best of our knowledge, there are few detailed investigations about the effects of catalyst characters on the photocatalytic activity and process of NiO catalyst in the degradation of organic dye.

In present work, for the purpose of obtaining series of NiO catalysts with different morphologies and sizes we chose four kinds of alkalis (namely sodium hydroxide NaOH, ammonia solution $NH_3{\cdot}H_2O$, urea $CO(NH_2)_2$, and triethanolamine $N(CH_2CH_2OH)_3$) to react with nickel nitrate $Ni(NO_3)_2$ to obtain NiO precursors and calcined the precursors at various temperatures to obtain NiO samlpes

* Corresponding author. Tel.: +86 20 39310187; fax: +86 20 39310187.
E-mail addresses: wanxia@scnu.edu.cn (X. Wan), tiesl@scnu.edu.cn (S.-l. Tie).
[1] Tel.: +86 20 39310187; fax: +86 20 39310187.

0169-4332/$ – see front matter © 2013 Elsevier B.V. All rights reserved.
http://dx.doi.org/10.1016/j.apsusc.2013.03.126

with different characters. With the help of SEM, XRD, BET, UV–vis, and PL analysis techniques, the effects of synthesis conditions on the characters of NiO samples were investigated. As a pholocatalyst in the degradation of methylene blue under UV-light irradiation, the effects of catalyst characters on the photocatalytic activity and degradation process of organism have been discussed extensively and the results possibly guid the purposive synthesis of catalyst.

2. Materials and experimental methods

2.1. Raw materials

The analytical reagents, nickel nitrate [$Ni(NO_3)_2{\cdot}6H_2O$], sodium hydroxide (NaOH), ammonia solution ($NH_3{\cdot}H_2O$), urea [$CO(NH_2)_2$], and triethanolamine [$N(CH_2CH_2OH)_3$] were purchased from Tianjin Damao Chemical Reagent Factory (Tianjin, China). Methylene blue (MB, ≥98.5%) and silver nitrate ($AgNO_3$, A.R.) were purchased from Tianjin Fine Chemical Development Centre (Tianjin, China). Methanol (MeOH) and anhydrous acetonitrile (CH_3CN) are of HPLC grade quality and purchased from Aladdin's Reagent Company Limited (Shanghai, China). All the chemicals in this study were used directly without further purification.

2.2. Synthesis of NiO nano-catalyst

By a hydrothermal process combining subsequent calcination the NiO catalysts were synthesized through the reactions of nickel nitrate with one of four kinds of alkalis, namely NaOH, $NH_3{\cdot}H_2O$, $CO(NH_2)_2$, and $N(CH_2CH_2OH)_3$, respectively. Typically, 80 mL of 1.2 mol L^{-1} alkali solution was slowly added into 80 mL of 0.6 mol L^{-1} $Ni(NO_3)_2$ solution at room temperature under stirring magnetically, afterwards the pH of cloudy suspension was adjusted to 8.0 by using HNO_3 or NaOH solution. The suspension was transferred into a 200 mL Teflon-lined stainless steel autoclave, sealed, then heated at 185 °C for 24 h in a furnace. After the reaction was complete, the steel autoclave was air-cooled down to room temperature. The resulting solid product was filtrated and washed with deionized water several times to remove the impurities. The product was dried in an oven at 80 °C for 24 h to obtain the precursor of NiO. These precursors are thermally treated at 400, 600, 800, and 1000 °C in air for 3 h, respectively, thus the NiO samples with various morphologies and particle sizes were obtained. The precursors obtained by using alkali reactants of NaOH, $NH_3{\cdot}H_2O$, $CO(NH_2)_2$, and $N(CH_2CH_2OH)_3$, respectively, were named A, B, C, and D. The NiO samples obtained by calcining A∼D precursors at 400, 600, 800, and 1000 °C, respectively, were named (A∼D)400, (A∼D)600, (A∼D)800, and (A∼D)1000 NiO.

2.3. Photocatalytic activity testing

In order to evaluate the photocatalytic activity of NiO, we use methylene blue (MB) as a model contamination to characterize the photocatalytic activity and process. A 125 W low-pressure mercury lamp predominantly emitting at 254 nm wavelength (produced by Philips Electronics Ltd.) was chosen as a irradiation source because the excited energy must higher or equal to the band gap E_g of NiO (about 3.5 eV). For each condition, 0.1 g of NiO catalysts were dispersed in 100 mL of 10 mg L^{-1} MB aqueous solution in darkness for 30 min to establish the adsorption equilibrium of MB. The initial pH of solution was adjusted at 6.5 for all experiments. The 250 mL beaker containing reactive solution was placed in a water bath which maintain temperature at 35 ± 0.2 °C. The photocatalytic reaction was carried out under UV-light irradiation from a 125 W UV lamp, which was positioned vertically 16 cm awary from the liquid surface in the beaker. After given time intervals, about 2 mL suspension was withdrawn by a syringe and filtered with a micropore filter (0.45 μm pore size). The filtrate was diluted and measured the absorbance at 655 nm wavelength (the maximum absorption wavelength of MB) on a UV–vis spectrophotometer to obtain the degradation rate of MB.

2.4. Analytic technique

The morphology and size of NiO sample were obtained by a field emission scan electron microscopy (JSM-6700F, Electron Company, Japan), and the crystal structure was determined by a XRD powder diffraction instrument (AXS D8-Advance, Bruker Company, Germany). The UV–vis absorption spectrum was measured on a UV–vis spectrophotometer (UV-1700, Shimadzu Corporation, Japan). The specific surface area of NiO sample was calculated from the BET adsorption equation and measured by the accelerated surface area porosimetry instrument (ASAP2010, Micromerities Company, USA) at liquid nitrogen temperature (77.4 K). Photoluminescence spectrum of NiO sample was obtained at room temperature on a fluorescent spectrometer (FLS920, Edinburgh Instruments, UK) with a xenon lamp as an excitation source.

3. Results and discussion

3.1. Effect of synthesis condition on the characters of NiO sample

3.1.1. Phase structure and particle size of NiO sample

The SEM images of as-prepared NiO samples A600, B600, C600, and D600 are shown in Fig. 1. A600 NiO obtained by using NaOH as a alkali shows a short rod shape, and the mean diameter and length are estimated at about 29 and 80 nm, respectively. B600 NiO obtained by using $NH_3{\cdot}H_2O$ as a alkali shows a wafer shape, and the mean diameter and length are estimated at about 250 and 350 nm, respectively. C600 and D600 NiO samples obtained by using $CO(NH_2)_2$ and $N(CH_2CH_2OH)_3$ as alkali reactants, respectively, show a cotton- and a flower-like shapes. These results implied that the chemical composition and base strength of alkali reactants observably affect both the compositions and morphologies of the obtained precursors, inducing the differences of as-prepared NiO samples in morphologies and sizes. In the reaction of Ni^{2+} ion with NaOH the concentration of OH^- in local region was correspondingly high due to the complete dissociation of NaOH, the crystal nucleus of the precursor [$Ni(OH)_2$] formed more rapidly and sufficiently, and the growth of $Ni(OH)_2$ crystallite was fast, then the precursor $Ni(OH)_2$ was obtained with a small size. In these NiO samples B600 exhibits the biggest particle size, good dispersity, high crystallinity, and smooth surface. When $NH_3{\cdot}H_2O$ solution was droped into $Ni(NO_3)_2$ solution, the $Ni(NH_3)_6^{2+}$ complex ions were formed firstly, then the decomposition of $Ni(NH_3)_6^{2+}$ ions at 185 °C induced the formation and growth of the precursor [$Ni(OH)_2$] slowly and regularly, so the $Ni(OH)_2$ with a bigger particle size and higher crystallinity was obtained. By calcining the precursor $Ni(OH)_2$ at 600 °C the B600 NiO sample with a wafer shape was obtained. The similar phenomenon has been found in the synthesis of D600 NiO sample because of the formation of $[Ni(OH)(N(CH_2CH_2OH)_3)]^+$ complex ion in the mixed solution of Ni^{2+} ion and $N(CH_2CH_2OH)_3$ alkali. Our experiments have proved that the precursor of urea ($CO(NH_2)_2$) reacting with Ni^{2+} ion at 185 °C was basic nickel carbonate $Ni_2(CO_3)(OH)_2$ and it decomposed ceaselessly from 50 to 550 °C to form NiO sample with a cotton-like when calcined the precursor at 600 °C. The particle size of NiO sample increase with increasing calcination temperature. When the precursor was calcined up to 800 °C, the obtained NiO sample began to melt, then totally melted and agglomerated each other at 1000 °C (the SEM images not been shown).

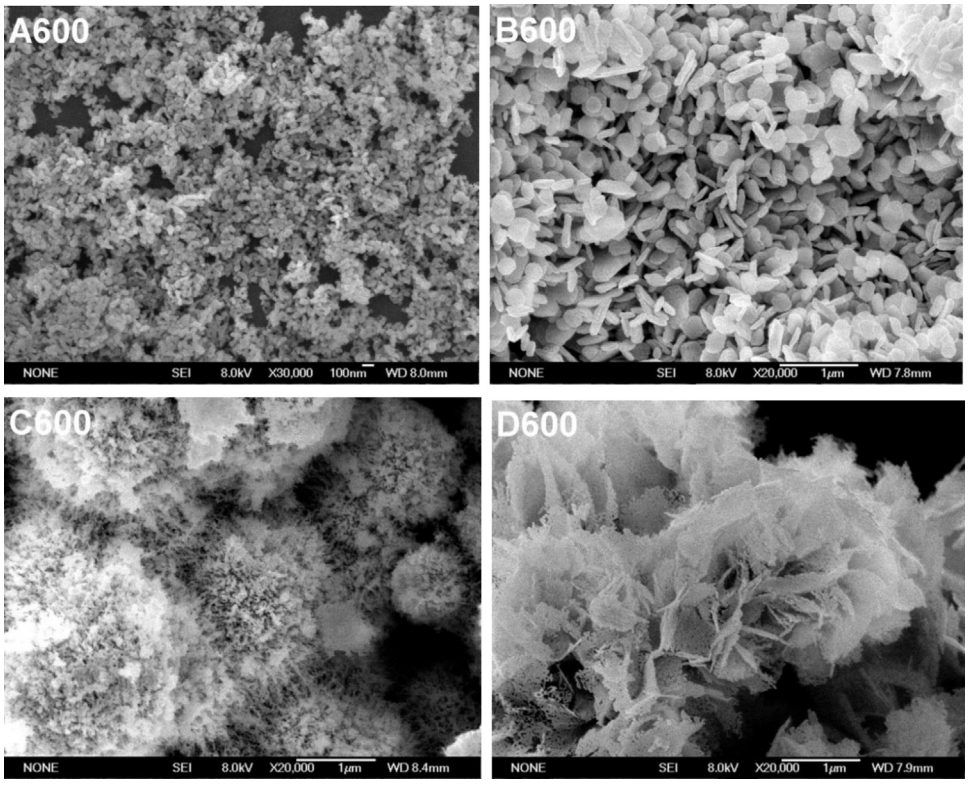

Fig. 1. SEM images of A600, B600, C600, and D600 NiO samples.

The XRD patterns of series of NiO samples synthesized by different alkali reactants and various calcination temperatures were shown in Fig. 2 and the average particle sizes of NiO samples calculated from the full-width half-maximum breadths of the (2 0 0) and (1 1 1) diffraction peaks using the Scherrer formula were presented in Table 1. It can be seen in Fig. 2 that for all as-prepared NiO samples, the diffraction peaks are well matched with that of bulk NiO (JCPDS, No. 78-0643) with a face centered cubic (FCC) crystal structure. The A600, B600, C600, and D600 NiO samples have high crystallinity and perfect crystal structures, and the average particle sizes calculated by the Scherrer formula were 26.7 nm, >100 nm, 28.6 nm, and 29.3 nm, respectively. When the precursor was calcined at low temperature (400 °C), the prepared NiO (A400) showed low and broad diffraction peaks due to the small size effect (about 10 nm) and imperfect crystal structure. When the precursor was calcined at 1000 °C, the prepared NiO (A1000) showed higher and sharper diffraction peaks, indicating the increase of particle size and the melting of crystal (according to the SEM result). Hence, the higher the calcination temperature, the larger the particle size, and the higher the crystallinity of NiO sample.

The BET surface areas of NiO samples are presented in Table 1. The result showed that A400 has the biggest BET surface area in all the NiO samples and the BET surface area of A1000 cannot be obtained accurately because of the melting and agglomerating of the sample. The BET surface areas of A600, B600, C600, and D600 samples were 18.7, 8.47, 12.7, and 9.80 $m^2 g^{-1}$, respectively. When the calcination temperature of the precursor increases from 400 to 800 °C, the BET surface areas of NiO samples (A400-A800) decrease from 125 to 4.52 $m^2 g^{-1}$. Hence, the larger the particle size, the smaller the BET surface area of NiO sample. According to SEM, XRD and BET analyses, the NiO sample prepared by using NaOH as a alkali reactant and calcined the precursor at 600 °C exhibits a perfect crystal structure, relatively small particle size, high crystallinity, and appropriate BET surface area. These characters would be beneficial for NiO catalyst to exhibit a high photocatalytic activity.

3.1.2. UV absorption property of NiO

Fig. 3 shows the UV–vis absorption spectra of NiO aqueous suspensions. It can be seen that the absorbances of NiO samples in UV region (200–400 nm) follow the trend: from A to D obtained at the same calcination temperature, A600 > C600 ≈ D600 > B600, and for A series with various calcination temperatures, A400 > A600 > A800 > A1000. The absorption of NiO in UV region decreases with increasing calcination temperature. The NiO sample with larger particle size and smaller surface

Table 1
Data of synthesis conditions, the characters of NiO samples, and the photocatalytic degradation rates of MB under 1 h UV-light irradiation.

Sample	Alkali reactant	Calcination temperature (°C)	Particle size d_{XRD}(nm)	BET surface area ($m^2 g^{-1}$)	Band gap E_g (eV)	MB degradation rate (%)
A600	NaOH	600	26.7	18.7	3.53	47.8
B600	$NH_3 \cdot H_2O$	600	250[a]	8.47	3.10	36.5
C600	$CO(NH_2)_2$	600	28.6	12.7	3.47	42.4
D600	$N(CH_2CH_2OH)_3$	600	29.3	9.80	3.27	40.6
A400	NaOH	400	10.0	125	3.67	37.2
A800	NaOH	800	52.2	4.52		41.2
A1000	NaOH	1000	>100	–		35.0

[a] Data comes from the SEM micrograph.

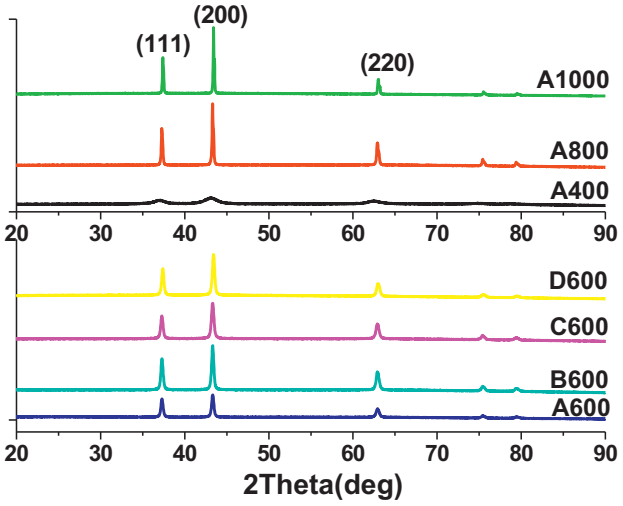

Fig. 2. XRD patterns of series of NiO samples synthesized by different alkaline reactants and different calcination temperatures.

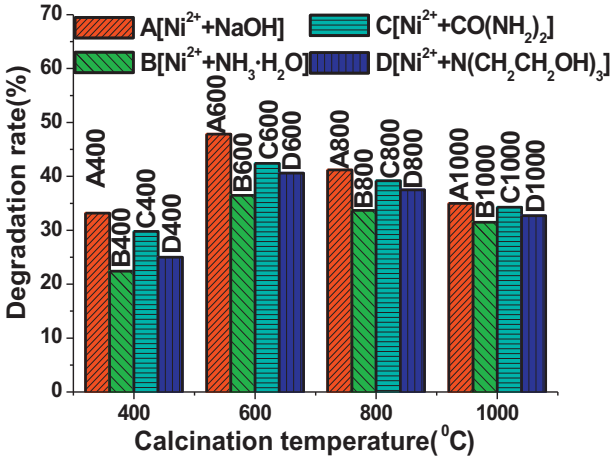

Fig. 4. Effects of the characters of NiO samples obtained from various synthesis conditions on the degradation rates of MB. Experimental conditions: [MB]: 10 mg L^{-1}, [NiO]: 1.0 g L^{-1}, pH: 6.5, temperature: 35 ± 0.2 °C, irradiation time: 60 min.

area, like B600, A800 and A1000 samples exhibits a very weak absorption in UV region. Consequently, the NiO sample which possesses a small particle size, rough surface, and high surface area has a strong ability to capture photons efficiently and exhibits a strong absorption in UV region.

In Fig. 3 the strong absorption of NiO sample in UV region results from the band gap absorption of NiO semiconductor. The absorption band gap E_g can be determined by the following equation [16,17]:

$$(ahv)^n = B(hv - E_g)$$

in which hv is the photo energy, α is the absorption coefficient, B is the constant related to the material and n is either 2 for a direct transition or 1/2 for an indirect transition. The extrapolation of the linear region of a plot of $(ahv)^2$ vs. hv gives the band gap E_g of semiconductor. According to the result of Fig. 3 the band gap E_{gs} of as-prepared NiO samples were measured and presented in Table 1. The result showed that NiO is a direct band gap semiconductor and the band gap E_g is about 3.5 eV [18]. The band gap E_g of NiO sample increases with the decrease of particle size due to a size quantization effect [19] and the absorption edge of NiO sample has a red shift with the increase of particle size [20].

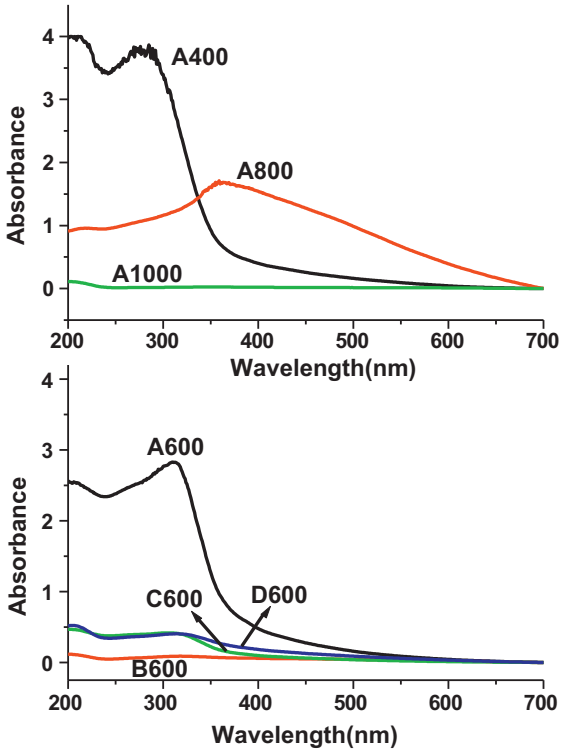

Fig. 3. UV–vis absorption spectra of NiO suspensions.

3.2. Effect of catalyst characters on photocatalytic activity and process

3.2.1. Effect of synthesis conditions on photocatalytic activity

The photocatalytic performances of NiO samples have been investigated by using methylene blue (MB) as a degradation substance. The blank experiment has proved that in the absence of NiO catalyst MB cannot be degraded under the irradiation of UV-light for 2 h. The degradation experiments were carried out under the condition: [MB]: 10 mg L^{-1}, [NiO]: 1.0 g L^{-1}, initial pH:6.5, reactive temperature: 35 ± 0.2 °C. The MB degradation rates of all the NiO samples were shown in Fig. 4. It showed that for A-D series of NiO samples calcined at the same temperature, the degradation rates follow the trend: A(400–1000) > C(400–1000) > D(400–1000) > B(400–1000). For same series of NiO samples calcined at various temperatures, the degradation rates follow the trend: (A–D)600 > (A–D)800 > (A–D)1000 > (A–D)400. Obviously, the synthesis conditions directly result in the differences of NiO characters and MB degradation rates. The effects of synthesis conditions and NiO characters on the degradation rates of MB were presented in Table 1. The results showed that A600 sample exhibits the highest degradation rate in all NiO samples. This is because A600 has a perfect crystal structure, smaller particle size, larger BET surface area, and stronger UV absorption than other NiO samples. The A400 sample which possesses the strongest UV absorption (shown in Fig. 3) and the largest BET surface area, but an imperfect crystal structure and poor crystallinity (showed widening XRD peaks in Fig. 2) exhibits a low degradation rate of MB. This result indicated that the integrality and regularity of NiO crystal structure have critical influences on the degradation rate because the photogenerated electron–hole pair was produced less on the surface of the catalyst which has a poor crystallinity and an imperfect crystal structure. Although the largest surface area and the strongest UV

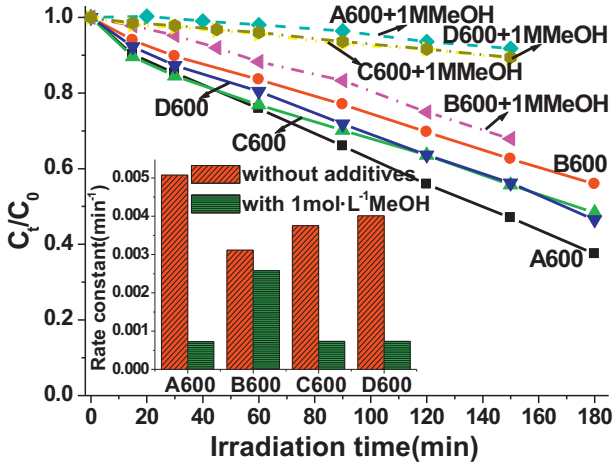

Fig. 5. Effect of MeOH on the photodegradation of MB in A~D600 NiO systems without and with 1.0 mol L^{-1} MeOH.

absorption of NiO catalyst can partially compensate the loss of photogenerated electron–hole pair. Therefore, under the condition of catalyst with a perfect crystal structure, the NiO sample which has a small particle size (<100 nm), large BET surface area, and strong UV absorption exhibits a high photocatalytic activity in the degradation of MB because these characters are beneficial for the catalyst to capture photons efficiently and generate electron–hole pairs in large quantities. According to the results of SEM, XRD, BET, and UV–vis analyses using NaOH as a alkali reactant can obtain the precursor with a small size, and calcined the precursor at 600 °C can obtain the NiO sample with a perfect crystal structure and appropriate particle size. Hence, for getting the NiO catalyst with a high photocatalytic activity, the optimal alkali reactant is NaOH and the optimal calcination temperature of the precursor is 600 °C.

3.2.2. *Effects of various solvents on photocatalytic process of MB*

It has been reported that alcohols, such as methanol (MeOH) are known $OH^{\bullet}$ radicals scavengers [21–23]. If $OH^{\bullet}$ radicals dominate the photocatalytic oxidation process of MB on NiO surface, the addition of MeOH would inhibit the reaction strongly. The effects of methanol on the degradation of MB in (A~D) 600 NiO suspensions without and with 1.0 mol L^{-1} MeOH were shown in Fig. 5. It has been validated that the photodegradation of MB follows a pseudo-first-order kinetics [24] and methanols exhibited intense influences on the degradation processes of MB in A600, C600, and D600 suspensions, but a little in B600 suspension. The results suggested that $OH^{\bullet}$ radicals play dominant roles in the degradation processes of MB in A600, C600, and D600 suspensions, but a small role in B600 suspension.

For understanding the different actions of $OH^{\bullet}$ radicals in A600 and B600 suspensions, the effects of solvents on the photodegradation of MB in A600 and B600 suspensions were shown in Fig. 6. The fact that the photodegradation of MB was intensively inhibited by MeOH suggested that on A600 catalyst surface MB was photooxidized by free $OH^{\bullet}$ radicals ($OH^{\bullet}_{free}$) and/or adsorbed $OH^{\bullet}$ radicals ($OH^{\bullet}_{ads}$) [25,26]. Further the fact that in an acetonitrile or in F^{-}-added A600 suspension the photodegradation of MB was intensively inhibited indicated that the forming of $OH^{\bullet}_{ads}$ radicals was minimized [16,27]. So in A600 suspension MB was photooxidized by $OH^{\bullet}_{ads}$ radicals.

In B600 suspension the rate constant of MB degradation slightly decreased from 3.99×10^{-3} min^{-1} in water to about 3.4×10^{-3} min^{-1} both in 1.0 mol L^{-1} MeOH and in 0.01 mol L^{-1} NaF, respectively, indicating the fact that $OH^{\bullet}$ radicals plays a small role during photocatalytic oxidation process [16]. If a substrate

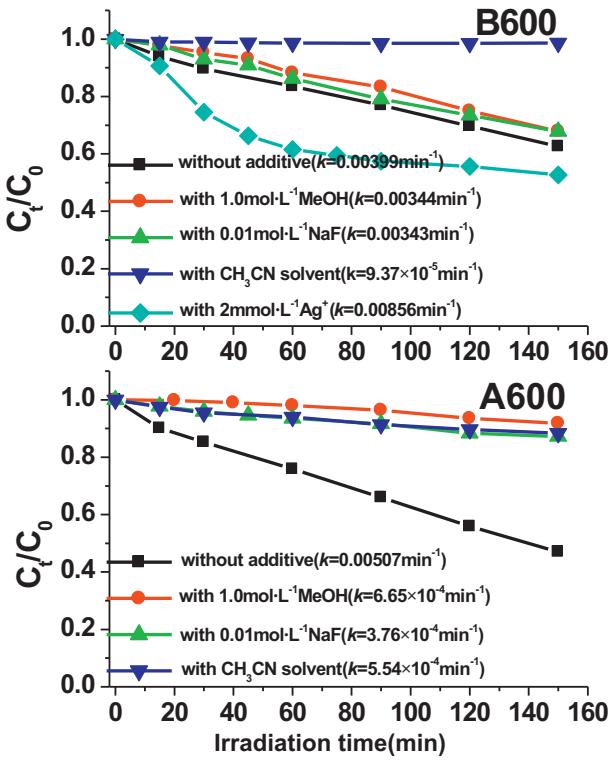

Fig. 6. Effects of solvents on the degradation of MB in A600 and B600 suspensions.

was being reduced by conduction band electron (e^{-}_{cb}), then the e^{-}_{cb} scavenger would inhibit the reaction. If a substrate was being oxidized, then the presence of e^{-}_{cb} scavenger could enhance its reaction rate by minimizing the rate of recombination of e^{-}_{cb} and h^{+}_{vb} [28]. Since Ag^{+} ion is an efficient e^{-}_{cb} scavenger [22], and the addition of 2 mmol L^{-1} Ag^{+} ions in a B600 suspension strikingly increased the photodegradation of MB ($k = 8.56 \times 10^{-3}$ min^{-1}). This result implies that in a B600 suspension MB was not being reduced by e^{-}_{cb}. On the other hand, the photodegradation of MB in an anhydrous solvent was completely inhibited ($k = 9.37 \times 10^{-5}$ min^{-1}), indicating the fact that photogenerated hole (h^{+}_{vb}) plays an important role in the photocatalytic process and the photooxidation of MB only occurred on the surface of catalyst [29].

Consequently, in A600, C600, and D600 NiO systems the photooxidation processes of MB occurred via the attack by $OH^{\bullet}$ radicals, and in B600 NiO system MB was oxidated by direct reacting with holes (h^{+}_{vb}).

3.2.3. *Effects of surface state and inner structure of catalyst on photocatalytic process of MB*

For understanding the differences in photocatalytic processes of MB between A–D series of NiO suspensions, the PL analysis of NiO samples were carried out at room temperature. It has been known that PL emissions of semiconductors result from the recombination of photo-induced charge carriers and the emissions are broadly divided into two categories: the band–band PL emission belonging to the electron transition from the conduction band (CB) bottom to the valence band (VB) top, and the excitonic PL emissions resulting from surface oxygen vacancies and defects of semiconductors [30,31]. For band–band PL emission, the lower the PL intensity, the higher the separation rate of photo-induced electron(e^{-}_{cb})-hole (h^{+}_{vb}) pair and, possibly, the higher the photocatalytic activity. For excitonic PL emissions, the relationships between PL intensity and photocatalytic activity are very complicated, which are dependent on the characters of semiconductors [32].

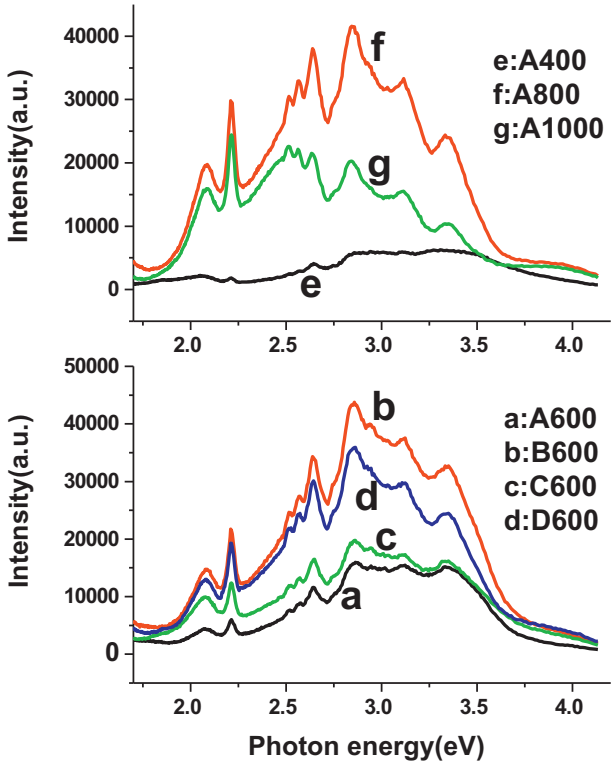

Fig. 7. Photoluminescence spectra of NiO samples (λ_{ex} = 254 nm).

Fig. 7 showed the PL spectra of NiO samples under 254 nm wavelength excitation at room temperature. The result showed that for all the NiO samples, the UV emission peaks at 3.35 eV (370 nm) are attributed to the exciton emissions from conduction band (e^-_{cb}) to valence band (h^+_{vb}). This result is in accord with the band gap E_g of NiO in Table 1. The result in Fig. 7 showed that the NiO sample with a higher crystallinity and a larger particle size shows a stronger band-band PL emission at 370 nm. The stronger the band-band PL intensity of NiO sample, the higher the recombination rate of photo-induced $e^-_{cb} - h^+_{vb}$ pair, then the lower the photodegradation rate of MB. B600 sample has the strongest band-band PL emission, so exhibits the lowest photodegradation rate of MB. The NiO sample with a higher crystallinity has a lower quantity of remanent chemical bonds on its surface to adsorb OH^- or H_2O radicals, inducing a low generation rate of $OH^\bullet$ radicals which come from the reaction of adsorbed OH^- or H_2O with hole ion (h^+_{vb}). In addition, the higher crystallinity of NiO sample induces a higher recombination rate of photo-induced $e^-_{cb} - h^+_{vb}$ pair. These factors induce NiO sample to exhibit a lower photodegradation rate of MB.

The prevenient studies have validated that in TiO_2 photocatalytic system there are two kinds of different trap sites for holes, the deep hole and the shallow hole. The deep hole exhibits an absorption around 520 nm, while the shallow hole exhibits an absorption around 1200 nm [33]. The shallowly trapped holes will therefore have comparable reactivity and mobility to free holes and react very rapidly with chemisorbed substances on the catalyst surface. The deeply trapped holes are more or less localized at deep traps, exhibit a lower oxidizing potential, and prefer to react with more mobile physisorbed substances [34,35]. As seen in Fig. 7, all the NiO samples showed several excitonic PL emission bands at 3.11 eV (398 nm), 2.86 eV (434 nm), 2.64–2.51 eV (470–493 nm), 2.22 eV (558 nm), and 2.08 eV (596 nm), respectively, resulting from the surface oxygen vacancies and defects of NiO samples [36]. Among them the yellow emissions at 2.22 and 2.08 eV are caused by diagonal transitions from the shallow donors in the potential valleys to unidentified deep acceptors in the potential hills [37]. The intensities of yellow emissions follow the trend: B600 > D600 > C600 > A600, demonstrating the fact that the number of deep level defects in NiO crystal lattice increases with the increasing of crystallinity and particle size of NiO sample. Hence, B600 has the greatest number of deep level defects in crystal lattice. These deeply trapped holes hardly react with chemisorbed oxhydryl OH^- or H_2O on NiO surface to generate $OH^\bullet$ radicals. So the NiO sample with a higher crystallinity and relatively smooth surface like B600 has more slightly active deeply trapped holes (h^+_{vb}) which were trapped on the NiO surface or migrated from the interior to the surface to react directly with physisorbed organism (MB) to be oxidized, inducing a low photocatalytic activity. Consequently, in B600 NiO system MB was oxidated by direct reacting with holes (h^+_{vb}). The NiO sample with relatively low crystallinity and rough surface like A600 has more active shallowly trapped holes to react very rapidly with chemisorbed oxhydryl OH^- or H_2O to generate $OH^\bullet$ radicals which could directly degrade MB to small molecules. So in A600, C600, and D600 NiO suspensions the photocatalytic degradation of MB occurred via the attack by $OH^\bullet$ radicals. Therefore, the surface states and inner structures of NiO catalysts show strong influences on the photocatalytic activities and processes in the degradation of MB.

4. Conclusions

The NiO nano-catalysts were synthesized via the hydrothermal reaction of nickel nitrate with one of four kinds of alkalis (namely sodium hydroxide, ammonia solution, urea, and triethanolamine) combining a subsequent calcination process. The characters of as-prepared NiO samples were investigated in detail and the effects of catalyst characters on the photocatalytic degradation of MB in UV/NiO system were discussed. The NiO samples obtained by using different alkali reactants showed the different characters in morphology and surface peculiarity, particle size, surface area, and crystallinity and crystal quality, exhibiting different performances in photocatalytic activity and process in UV/NiO system. The NiO samples obtained by calcined the same precursor at different temperatures showed the different characters in crystallinity and crystal quality, particle size, and surface area, only exhibiting the different performance in photocatalytic activity. On the premise of catalyst with a perfect crystal structure, the photocatalytic activity of NiO catalyst increases with the decrease of particle size, the increase of BET surface area, and the enhancement of UV absorption. According to the attribute of PL emission, the stronger the PL intensities of yellow emissions at 2.22 and 2.08 eV, the more the number of deep level defects in NiO crystal lattice, and the lower the photocatalytic activity of NiO sample. Consequently, the NiO sample which has a good crystallization and small particle size (<100 nm) possesses more shallowly trapped holes to react with chemisorbed oxhydryl OH^- or H_2O to generate $OH^\bullet$ radicals, inducing a high photocatalytic activity, furthermore, in this UV/NiO suspension the photocatalytic oxidation process of MB occurrs via the attack by $OH^\bullet$ radicals. The NiO sample which has a higher crystallization and a bigger particle size (>200 nm) possesses more deeply trapped holes (h^+_{vb}) to react directly with physisorbed organism to be oxidized, inducing a low photocatalytic activity, therefore, in this system the MB is oxidized by direct reacting with holes (h^+_{vb}).

Acknowledgements

This work was supported by Nano-Project of Guangzhou City (2007Z3-D2041) and the project for high-level professionals in the Universities of Guangdong Province, People's Republic of China.

References

[1] K. Vignesh, A. Suganthi, M. Rajarajan, R. Sakthivadivel, Visible light assisted photodecolorization of eosin-Y in aqueous solution using hesperidin modified TiO_2 nanoparticles, Applied Surface Science 258 (2012) 4592–4600.

[2] Y.S. Liu, J. Han, W. Qiu, W. Gao, Hydrogen peroxide generation and photocatalytic degradation of estrone by microstructural controlled ZnO nanorod arrays, Applied Surface Science 263 (2012) 389–396.

[3] S.L. Wang, P.G. Li, H.W. Zhu, W.H. Tang, Controllable synthesis and photocatalytic property of uniform CuO/Cu_2O composite hollow microspheres, Powder Technology 230 (2012) 48–53.

[4] F.A. Harraz, R.M. Mohamed, A. Shawky, I.A. Ibrahim, Composition and phase control of Ni/NiO nanoparticles for photocatalytic degradation of EDTA, Journal of Alloys and Compounds 508 (2010) 133–140.

[5] E. Dvininov, M. Ignat, P. Barvinschi, M.A. Smithers, E. Popovici, New SnO_2/MgAl-layered double hydroxide composites as photocatalysts for cationic dyes bleaching, Journal of Hazardous Materials 177 (2010) 150–158.

[6] Y.P. Sun, C.J. Murphy, K.R. Reyes-Gil, E.A. Reyes-Garcia, J.P. Lilly, D. Raftery, Carbon-doped In_2O_3 films for photoelectrochemical hydrogen production, International Journal of Hydrogen Energy 33 (2008) 5967–5974.

[7] A. Fujishima, X.T. Zhang, D.A. Tryk, TiO_2 photocatalysis and related surface phenomena, Surface Science Reports 63 (2008) 515–582.

[8] T. Daimon, T. Hirakawa, M. Kitazawa, J. Suetake, Y. Nosaka, Formation of singlet molecular oxygen associated with the formation of superoxide radicals in aqueous suspensions of TiO_2 photocatalysts, Applied Catalysis A-General 340 (2008) 169–175.

[9] Y.X. Chen, S.Y. Yang, K. Wang, L.P. Lou, Role of primary active species and TiO_2 surface characteristic in UV-illuminated photodegradation of Acid Orange 7, Journal of Photochemistry and Photobiology A 172 (2005) 47–54.

[10] S. Boumaza, A. Belhadi, M. Doulache, M. Trari, Photocatalytic hydrogen production over NiO modified silica under visible light irradiation, International Journal of Hydrogen Energy 7 (2012) 4908–4914.

[11] C. Hu, X.X. Hu, J. Guo, J.H. Qu, Efficient destruction of pathogenic bacteria with $NiO/SrBi_2O_4$ under visible light irradiation, Environmental Science and Technology 40 (2006) 5508–5513.

[12] P.W. Pan, Y.W. Chen, Photocatalytic reduction of carbon dioxide on $NiO/InTaO_4$ under visible light irradiation, Catalysis Communications 8 (2007) 1546–1549.

[13] T. Sreethawong, S. Ngamsinlapasathian, S. Yoshikawa, Surfactant-aided sol–gel synthesis of mesoporous-assembled TiO_2–NiO mixed oxide nanocrystals and their photocatalytic azo dye degradation activity, Chemical Engineering Journal 192 (2012) 292–300.

[14] C.J. Chen, C.H. Liao, K.C. Hsu, Y.T. Wu, J.C.S. Wu, P–N junction mechanism on improved NiO/TiO_2 photocatalyst, Catalysis Communications 12 (2011) 1307–1310.

[15] Z.Y. Zhang, C.L. Shao, X.H. Li, C.H. Wang, M.Y. Zhang, Y.C. Liu, Electrospun nanofibers of p-type NiO/n-type ZnO heterojunctions with enhanced photocatalytic activity, ACS Applied Materials & Interfaces 2 (2010) 2915–2923.

[16] D. Adler, J. Feinlieb, Electrical and optical properties of narrow-band materials, Physical Review B 2 (1970) 3112–3134.

[17] D.K. Schroder, Semiconductor Material Device Characterisation, Wiley, New York, 1998.

[18] G. Boschloo, A. Hagfeldt, Spectroelectrochemistry of nanostructured NiO, Journal of Physical Chemistry B 105 (2001) 3039–3044.

[19] E. Burstien, Anomalous Optical Absorption Limit in InSb, Physical Review 93 (1954) 632–633.

[20] N. Talebian, M.R. Nilforoushan, Comparative study of the structural, optical and photocatalytic properties of semiconductor metal oxides toward degradation of methylene blue, Thin Solid Films 518 (2010) 2210–2215.

[21] O. Mekasuwandumrong, P. Pawinrat, P. Praserthdam, J. Panpranot, Effects of synthesis conditions and annealing post-treatment on the photocatalytic activities of ZnO nanoparticles in the degradation of methylene blue dye, Chemical Engineering Journal 164 (2010) 77–84.

[22] M.R. Hoffmann, S.T. Martin, W. Choi, D.W. Bahnemann, Environmental applications of semiconductor photocatalysis, Chemical Reviews 95 (1995) 69–96.

[23] I. Ilisz, A. Dombi, Investigation of the photodecomposition of phenol in near-UV-irradiated aqueous TiO_2 suspensions. II. Effect of charge-trapping species on product distribution, Applied Catalysis A-General 180 (1999) 35–45.

[24] K. Hayat, M.A. Gondal, M.M. Khaled, S. Ahmed, Effect of operational key parameters on photocatalytic degradation of phenol using nano nickel oxide synthesized by sol–gel method, Journal of Molecular Catalysis A 336 (2011) 64–71.

[25] S. Kanecoa, N. Li, K.K. Itoh, H. Katsumata, T. Suzuki, K. Ohta, Titanium dioxide mediated solar photocatalytic degradation of thiram in aqueous solution: kinetics and mineralization, Chemical Engineering Journal 148 (2009) 50–56.

[26] N. Daneshvar, D. Salari, A.R. Khataee, Photocatalytic degradation of azo dye acid red 14 in water on ZnO as an alternative catalyst to TiO_2, Journal of Photochemistry and Photobiology A 162 (2004) 317–322.

[27] N. Serpone, E. Pelizzetti, H. Hidaka, in: D.F. Ollis, H. Al-Ekabi (Eds.), Photocatalytic Purification and Treatment of Water and Air, Elsevier Science, New York, 1993, pp. 225–250.

[28] M.M. Halmann, Photodegradation of Water Pollutants, New York, CRC Press, 19967–17.

[29] C.S. Turchi, D.F. Ollis, Photocatalytic degradation of organic water contaminants: mechanisms involving hydroxyl radical attack, Journal of Catalysis 122 (1990) 178–192.

[30] M.H. Zhou, J.Q. Yu, S.W. Liu, P.C. Zhai, L. Jiang, Effects of calcination temperatures on photocatalytic activity of SnO_2/TiO_2 composite films prepared by an EPD method, Journal of Hazardous Materials 154 (2008) 1141–1148.

[31] L. Dai, X.L. Chen, W.J. Wang, T. Zhou, B.Q. Hu, Growth and luminescence characterization of large-scale zinc oxide nanowires, Journal of Physics: Condensed Matter 15 (2003) 2221–2226.

[32] L.Q. Jing, Y.C. Qu, B.Q. Wang, S.D. Li, B.J. Jiang, L.B. Yang, W. Fu, H.G. Fu, J.Z. Sun, Review of photoluminescence performance of nano-sized semiconductor materials and its relationships with photocatalytic activity, Solar Energy Materials and Solar Cells 90 (2006) 1773–1787.

[33] T. Yoshihara, R. Katoh, A. Furube, Y. Tamaki, M. Murai, K. Hara, S. Murata, H. Arakawa, M. Tachiya, Identification of reactive species in photoexcited nanocrystalline TiO_2 films by wide-wavelength-range (400–2500 nm) transient absorption spectroscopy, Journal of Physical Chemistry B 108 (2004) 3817–3823.

[34] D.W. Bahnemann, M. Hilgendorff, R. Memming, Charge carrier dynamics at TiO_2 particles: reactivity of free and trapped holes, Journal of Physical Chemistry B 101 (1997) 4265–4275.

[35] Y. Tamaki, A. Furube, M. Murai, K. Hara, R. Katoh, M. Tachiya, Direct observation of reactive trapped holes in TiO_2 undergoing photocatalytic oxidation of adsorbed alcohols: evaluation of the reaction rates and yields, Journal of the American Chemical Society 128 (2006) 416–417.

[36] M.H. Zhou, J.G. Yu, S.W. Liu, P.C. Zhai, L. Jiang, Effects of calcination temperatures on photocatalytic activity of SnO_2/TiO_2 composite films prepared by an EPD method, Journal of Hazardous Materials 154 (2008) 1141–1148.

[37] M.A. Reshchikov, V. Avrutin, N. Izyumskaya, R. Shimada, H. Morkoc, Anomalous shifts of blue and yellow luminescence bands in MBE-grown ZnO films, Physica B 401–402 (2007) 374–377.